Supporting Online Material for

Conformational Spread as a Mechanism for Cooperativity in the Bacterial Flagellar Switch

Fan Bai, Richard W. Branch, Dan V. Nicolau Jr., Teuta Pilizota,
Bradley C. Steel, Philip K. Maini, Richard M. Berry*

*To whom correspondence should be addressed. E-mail: r.berry1@physics.ox.ac.uk

Published 5 February 2010, *Science* **327**, 685 (2010)
DOI: 10.1126/science.1182105

This PDF file includes:

Other Supporting Online Material for this manuscript includes the following:
(available at www.sciencemag.org/cgi/content/full/327/5966/685/DC1)

Supporting Online Material

Table of contents

A) Materials and methods

1. Experimental Procedure and Data Acquisition

1.1 Back focal plane interferometry

Polystyrene beads (diameter 0.5 μm; Polysciences) were attached to truncated flagella of immobilized *E. coli* cells (strain KAF84 (*fliC726*, pilA'-kan), pFD313 (*fliC*st, Ap^{R}) (*S1*)) in custom flow chamber slides. Cells were grown aerobically from frozen stocks for 5 h at 30 °C, in tryptone broth (TB) containing antibiotics to preserve plasmids. Bead position (*x*, *y*) was measured by back-focal-plane laser interferometry using a 633 nm Helium-Neon laser, anti-alias filtered at 4 kHz, and sampled at 10 kHz as described (*S2*). Custom QuView software allowed real-time monitoring of the bead spatial trajectory and beads with steady elliptical or circular trajectories were recorded. Each cell was recorded for 30 s only, to avoid cumulative laser damage and natural variability in bias (*S3*, *S4*). Measurements were taken from a single slide for no longer than three hours. All experiments were performed at 23 °C.

1.2 Resolution

The relaxation time of a 532nm bead attached to an elastic hook rotating about an axis 150nm from its diameter is about 1.1 ms (*S5*) (the lower limit of time resolution assuming no contribution from the flagellar stub (*S6*)) and the setup provides an angular resolution of 1°.

1.3 Categorizing cells by bias

The CW bias was calculated for each 30 s cell record as the fraction of the record spent in the CW state as determined through interval measurement (see section 2.3). Bias was observed to vary across the cell population, spanning the entire CW bias range. To increase the yield of cells in higher CW bias bins, attractant removal was applied to a subset of slides to stimulate chemotactic behaviour (*S7*). Motility buffer (10 mM

Potassium phosphate, 0.1 mM EDTA at pH 7.0) containing an attractant mixture (1 mM attractant (10μM L-aspartate, 1mM L-serine)) was injected into the flow chamber and measurements were taken for up to 10 minutes. The mixture was then flushed out with plain motility buffer and measurements were taken for up to 10 minutes. Flow chambers allowed a complete exchange of medium in about 5 s. This protocol was repeated for the duration of the experiment.

1.4 Obtaining instantaneous motor speed

Each sampled bead position, recorded as an (*x*, *y*) pair, was converted into an angle and a radius by fitting an ellipse to the bead trajectory (*S8*), and assuming that trajectories represent the projection of circular orbits onto the focal plane of the microscope (*S2*). Angles were converted to instantaneous motor speed by dividing the difference between successive angles by the sampling time, 0.1 ms. To reduce noise, the record of speed *vs.* time was 100 point median filtered before further analysis.

2. Analyzing Switching

2.1 Histogram of speeds

A histogram of filtered speeds in each filtered 30 s speed record was constructed, with bins 0.1 Hz wide. Speed histograms typically showed two peaks, one each for the CW and CCW rotation modes. A Gaussian fit to the outer half of each peak was used to obtain the mean CCW and CW speeds, μ_{CCW} and μ_{CW}, and the corresponding standard deviations, σ_{CCW} and σ_{CW}. This fitting was achieved in two steps: for the CCW peak, a preliminary Gaussian fit was made to the data range greater than 20 Hz to provide a mean and standard deviation; a second Gaussian fit was then made to the data range greater than this mean minus a quarter of the standard deviation.

2.2 Measuring complete switch durations

2.2.1 Criteria for selection

In order to ensure that data analyzed were attributable to the motor itself rather than extraneous factors, we analyzed only data that satisfied the following criteria. Data from an individual cell were analyzed for switching only if the speed histogram exhibited two modes that could be automatically and accurately fit as described (see section 2.1). Then, in order to ensure that each measured switch duration reflects the activity on the ring, a histogram was constructed of the measured radii of all points in the bead trajectory. Only records exhibiting unimodal histograms (judged by visual inspection) were considered, excluding beads that were not stably attached to motors. In addition, after switch duration measurement (section 2.2.2), the radius of the bead trajectory through the measured switch was checked to ensure a tight coupling between bead and motor activity. A

Gaussian fit was applied to the radius histogram for the entire 30 s record containing the switch. The radius during the switch was monitored from 10 points before the beginning of, to 10 points after the end of, the switch event. The switch was accepted if the radius during the switch was never beyond two standard deviations from the mean of the Gaussian fit to the radius histogram for the entire record.

2.2.2 Duration measurement

Complete switches were detected by a custom-written algorithm encoded in MATLAB (The MathWorks, Inc.). CCW and CW thresholds were defined as $\alpha_{CCW} = \alpha\mu_{CCW}$ and $\alpha_{CW} = \alpha\mu_{CW}$ with the parameter α set to 2/3. Complete switch events were located by searching for successive crossings of both thresholds in the same direction in the median-filtered speed record (Fig. S10). The direction of crossing was used to label the direction of the switch. The midpoint in time of the threshold crossings was saved as the centre point of the complete switch event.

The temporal location of the centre point of a complete switch was used to locate the switch event in the unfiltered, high resolution record of bead-angle *vs.* time. A switch event in the angle *vs.* time record comprises a linear component corresponding to smooth rotation in the preceding direction, followed by a central region corresponding to deceleration, reversal and acceleration in the opposite direction, and finally another linear component corresponding to smooth rotation in the following direction.

Two 20-point (2 ms) running windows were set to run outwards from the centre point in the bead-angle record. The CCW (CW) window continues until both (a) the slope of a linear fit to the points in the window is above (below) α_{CCW} (α_{CW}), and (b) the root-mean-square error (RMSE) of the linear fit is within the noise profile of the CCW (CW) state.

The noise profile of the CCW (CW) state was defined as follows. A 20-point running window was passed through the entire 30 s bead-angle record (totaling 30 s × 10 kHz = 300,000 points) and a linear fit obtained for each position of the window. A "noise histogram" was constructed containing the RMSEs of all the linear fits. The shape of the noise histograms deviated slightly from a Gaussian function, with relatively long tails in the direction of high noise that we attribute to switching and incomplete switching events in the record. As in section 2.1, we fitted the inner portion of the noise histogram with a Gaussian function and defined this curve as the noise profile of the CCW (CW) state, which is attributed to Brownian motion, the fluctuations produced by the fundamental stepping mechanism, and instrumental noise. If the RMSE of the linear fitting of the window in (b) at a certain position was further than three standard deviations from the mean of the noise profile, we concluded this position was still within a switch event. Since the noise profile varies slightly from cell to cell, noise profile construction was repeated for each record.

Finally, the switch duration was defined as the interval between the inner extremes of the stopped windows. The choice of window size is important: too short and the window

lacks statistical accuracy; too long and it is not sensitive to the local change of slope and RMSE. A 20-point (2 ms) window was found to provide an accurate measurement compared to the switch time determined by visual examination of the angular position record and is robust to variations of ±5 points (0.5 ms).

2.2.3 Correlation between switch duration and angular position

The average magnitude of the correlation coefficient between switch duration and the angle at which a switch begins, assessed for each record with at least ten measured switch events (a total of 80 records), was 0.20.

To assess the significance of this correlation, we generated 100 sets of 10-20 pairs of uncorrelated switch durations and angles, each representing a simulated 30 second record. We drew durations from a gamma distribution that fit the experimental switch duration distribution and switch angles from a uniform distribution. The magnitude of the correlation coefficient was calculated for each set, and the average correlation coefficient over the 500 sets calculated for comparison with the experimental correlations. This was repeated fifty times, giving an estimate of 0.20 ± 0.02 for the magnitude of the average correlation coefficient due to sampling alone. This is similar to the equivalent experimental value, indicating no true correlations.

2.3 Complete and incomplete switch interval measurement

2.3.1 Criteria for 30 s records used for interval measurement

In order to ensure that data analyzed were attributable to the motor itself rather than extraneous factors, we analyzed only data that satisfied the following criteria. Data from an individual cell were analyzed for switching only if the speed histogram exhibited two modes that could be automatically and accurately fit as described (see section 2.1). Then, to ensure accurate interval measurement, all records in which beads may have been perturbed by their local environment were excluded as follows. Pauses due to sticking would be expected to occur at the same angle on successive revolutions, whereas those due to incomplete switching would be randomly distributed. We therefore excluded all records where pauses were found at angles which were inconsistent with a random distribution of pause angle. In each 30 s filtered speed record, pauses were defined as incomplete switches detected using a threshold $\beta = 0.1$ but not detected using a threshold $\beta = -0.1$ (see section 2.3.4). The maximum number of pauses, k, detected in a 45^o bin swept in 1^o increments around the orbit was determined. k was subjected to a binomial test with $p\text{-}value = f(k: n, q)$, where n is the total number of incomplete switches located and, with the hypothesis of uniformly randomly distributed pausing angles, $q = 45/360$. A confidence level of 0.01 was used.

2.3.2 Complete switch interval measurement

Downward passages across the threshold α_{CW} marked the end of a CCW interval and the beginning of a CW interval while upward passages across α_{CCW} marked the end of a CW interval and the beginning of a CCW interval (Fig. S10).

2.3.3 Criteria for incomplete switch interval measurement

Those records accepted for analysis in section 2.3.1 were used here. Detection of incomplete switches is sensitive to both the magnitude of the noise in the speed record and variations in motor speed due to short-term de-energisation and stator changes. To reduce false incomplete switch detection, incomplete switches were searched for within a particular CCW or CW interval only if that interval satisfied the following criteria.

a) The interval was long enough to allow automated Gaussian fitting of the outside portion of the speed histogram, as described in section 2.1, to obtain the mean μ and standard deviation σ of the speed during the interval.

b) The speed noise in the interval was small compared to the threshold for defining incomplete switches; specifically $\mu - 2\sigma > \beta$, where β was the threshold parameter for detection of incomplete switches (see section 2.3.4).

c) Speed variations (on a slower time-scale) were small. To measure motor speed variation, a *0.5 s* window was ran across the interval (in *0.1 s* increments) with Gaussian fitting undertaken at each step to provide a set of window mean speeds μ_i. The episode was deemed stable if the range of μ_i was less than 2σ.

This approach resulted in incomplete switch detection that agreed with visual inspection.

2.3.4 Incomplete switch interval measurement

Incomplete switches were detected in a similar way to complete switches, using the additional CCW and CW thresholds $\beta_{CCW} = \beta\mu_{CCW}$ and $\beta_{CW} = \beta\mu_{CW}$, with $\beta < \alpha$. Incomplete switch events within a CCW interval were located by searching for a crossing of β_{CCW} followed by a crossing of α_{CCW}, corresponding to a transient reduction of speed by at least the factor of β (Fig. S10). For the analysis of intervals between incomplete switches we used $\beta = 1/3$. Similarly, incomplete switch events within a CW interval were located by searching for a crossing of β_{CW} followed by a crossing of α_{CW}. The later of the two threshold crossings was saved as the location of the incomplete switch event.

3. Model simulations

3.1 General description of the conformational spread model

The conformational spread model is used here to simulate the behaviour of the switch complex, consisting of 34 identical protomers arranged as a ring. Each protomer has two properties: (1) It is either in an *active* (**A**) or *inactive* (**a**) conformation, and (2) it may be bound (**B**) or not bound (**b**) to a single CheY-P molecule. This allows each protomer to undergo transitions between four possible states, **AB↔Ab↔ab↔aB↔AB**. The model assumes that the rate constants for a single protomer undergoing a change in activity (i.e. **AB↔aB** or **Ab↔ab**) are affected by the conformation of the two adjacent protomers, but that the rate constants for CheY-P binding to a protomer are affected only by the conformation of the protomer itself. Since each neighboring protomer may be either active or inactive, this leads to four sets of rate constants for each of these transitions. The general model of conformational spread thus consists of 10 possible reversible transitions for each protomer, and 20 associated rate constants, 16 of which can be independently set with the final four fixed by a consideration of detailed balance.

We have investigated a subspace of this general model, which we term the symmetrical model. It is defined by the following points:
i. There is no preferred direction in the ring, so a protomer with one adjacent protomer active, and the other inactive, will be unaffected if both adjacent protomers were to switch conformation.
ii. For a protomer with exactly one active adjacent protomer, binding a CheY-P molecule shifts the energetically favoured conformation from inactive to active, with equal favoritism in each case. That is, $\Delta G(\mathrm{AB} \rightarrow a\mathrm{B}) = \Delta G(\mathrm{ab} \rightarrow Ab) > 0$. We use E_A to represent the free energy on the left of this equation.
iii. For each protomer adjacent to a protomer of different conformation, the Gibbs free energy of the system increases by an amount E_J. Thus, for example, a protomer adjacent to two inactive protomers, the transition from active to inactive is thermodynamically favoured by $2E_J$ in addition to the free energy difference from (ii).
iv. Rate constants for conformational change are expressed as:

$$k_{a\rightarrow A} = \omega_a \exp\left(\frac{\lambda_a}{k_b T}\Delta G(\mathrm{a} \rightarrow \mathrm{A})\right)$$

$$k_{A\rightarrow a} = \omega_a \exp\left(\frac{\lambda_a - 1}{k_b T}\Delta G(\mathrm{a} \rightarrow \mathrm{A})\right)$$

Consistent with previous modeling of the switch complex, we chose to use $\omega = 10^4\ s^{-1}$ as a typical rate for conformational changes (*S9, S10*). Lacking information about lambda, we used an intermediate $\lambda = 0.5$. ΔG is calculated from (ii-iii), and holds one of six values: $\pm E_A$, $\pm(E_A+2E_J)$ or $\pm(E_A-2E_J)$.

v. The free energy associated with CheY-P binding depends only on the conformation of the protomer bound, and not on adjacent protomers. Binding rates are expressed as:

$$k_{b\to B} = \frac{c}{c_{0.5}}\omega_b \exp\left(\frac{\lambda_b}{kT}\Delta G^*(\mathrm{b}\to\mathrm{B})\right)$$
$$k_{B\to b} = \omega_b \exp\left(\frac{\lambda_b - 1}{kT}\Delta G^*(\mathrm{b}\to\mathrm{B})\right)$$

where c is the concentration of CheY-P, $c_{0.5}$ is the concentration of CheY-P required for neutral bias, and $\Delta G^*(\mathrm{b}\to\mathrm{B})$ is the free energy associated with binding when CheY-P is at the concentration $c_{0.5}$. We chose $\omega = 10\ s^{-1}$ based on the experimentally determined CheY-P binding rate (*S11*), and consistent with previous modeling of the switch complex (*S9, S12*), and $\lambda = 0$ such that the binding rate is independent of protomer conformation. The free energy of CheY-P binding is:

$$\Delta G(\mathrm{b}\to\mathrm{B}) = \Delta G^*(\mathrm{b}\to\mathrm{B}) - \log_e\left(\frac{c}{c_{0.5}}\right) = -\log_e\left(\frac{c}{c_{0.5}}\right) \pm E_A$$

This enables the free energy diagram from Fig. 1B of the main text to be redrawn in the case of $c \neq c_{0.5}$, as shown in figure S11.

3.2 A summary of the symmetric model

We consider the switch complex to be a ring of 34 identical protomers, each consisting of ~1 FliG, 1 FliM and a tetramer of FliN subunits. Each protomer possesses a single binding site, to which a CheY-P molecule can be bound (**B**) or not bound (**b**). Each protomer can independently exist in each of two conformations, *active* (**A**, corresponding to CW rotation) or *inactive* (**a,** CCW). It is assumed that CheY-P binds the active state more strongly.

A free energy diagram of the four resulting states of a protomer (**AB**, **aB**, **Ab**, **ab**), and the transitions between them, is shown in Fig. 1B for the case of CW bias = 0.5. Without CheY-P bound the inactive (CCW) state is energetically favoured, and with CheY-P bound the active (CW) state is favoured, consistent with the known relationship between bias and CheY-P concentration (*S10*). For simplicity we consider the symmetrical case where the magnitude of the free energy difference between favoured and unfavoured states (E_A) is the same with or without CheY-P bound.

Each protomer interacts with adjacent protomers in a way that favours pairs with the same conformation. We assume the free energy of interaction is independent of CheY-P binding, and is lower by E_J per protomer for any like-pair compared to any unlike-pair.

These interactions add 0, $+2E_J$ or $-2E_J$ to the free energy of a conformational change, depending upon the state of adjacent protomers (Fig. 1C).

The values of E_A and E_J govern the mechanisms by which conformational change can spread around the ring. As E_A becomes large, binding of CheY-P correlates precisely with activity state – that is, states **aB** and **Ab** are rarely occupied. The limit of very large E_A gives behaviour equivalent to the sequential model of allosteric regulation, where coupling between ligand binding and conformation is absolute.

At low values of E_J, the ring exhibits a random pattern of states as the protomers flip independently of each other. As the interaction between adjacent protomers is strengthened, domains of like conformational state dominate, until past a critical value of E_J the behaviour becomes switch-like (*S4*): the ring spends the majority of time in a coherent state, stochastically switching between CCW and CW configurations. Switches typically occur via a single nucleation of a new domain, followed by conformational spread of the domain, which follows a biased random walk until it either encompasses the entire ring, or collapses back to the previous coherent state (Fig. 1D, Movie S1). In the limit of very large E_J values, adjacent protomers are energetically forbidden from holding different conformations, leading to behaviour equivalent to the concerted model of allosteric regulation where all subunits switch simultaneously.

To simulate the conformational spread model, we calculated rate constants for CheY-P binding using

$$k_{b\to B} = \left(\frac{c}{c_{0.5}}\right)\omega_b$$

$$k_{B\to b} = \omega_b \exp\left(\frac{\Delta G^*_{B\to b}}{k_B T}\right)$$

where ω_b is the characteristic binding rate, $c/c_{0.5}$ is the concentration of CheY-P relative to that required for bias = 0.5 and $\Delta G^*_{B\to b}$ is the free energy difference of unbinding at $c = c_{0.5}$ (= $\pm E_A$, see above and Fig. 1B). We calculated rate constants for conformational change of the protomers using

$$k_{ij} = \omega_a \exp\left(-\frac{\Delta G_{ij}}{2k_B T}\right)$$

where ω_a is the characteristic rate of conformational changes, and the free energy difference of a transition from state i to state j, ΔG_{ij}, includes the effects of binding energy (Fig. 1B) and interactions (Fig. 1C). A more general description of the parameters of the conformational spread model is given in section 3.1 above.

3.3 Monte-Carlo simulation of conformational spread

C++ was used to generate a Monte-Carlo simulation of the conformational spread model. Each protomer is initially set to inactive and without CheY-P bound (note that interval analysis begins only from the first switch, so any initial perturbation of behaviour due to initial conditions will not affect the final analysis). Following on from initial conditions, each protomer *n* of the ring is assigned two transition times, A_n and B_n, at which it will undergo a state change associated with (A) activation or inactivation and (B) binding or release of CheY-P. The rate constants *k* for each transition are as specified in section 3.2, and the time for each forthcoming transition was calculated as $t\text{-}t_0 = -log_e(rand)/k$, where t_0 is the simulation time at which the calculation is made and *rand* is a random number (8 byte double) generated in the interval 0 to 1 according to the Mersenne-twister algorithm (*S13*).

The simulation iteratively progresses to the earliest time present in the arrays *A* and *B*, and modifies the state of the corresponding protomer accordingly. New transition times A_n and B_n are then calculated for that protomer, and, if the transition was associated with a change in activity of that protomer, then transition times A_{n+1} and A_{n-1} for the two neighboring protomers are also recalculated.

The number of active protomers and bound CheY-P were recorded at times $m\Delta t$, for integer *m* up to 300,000 and Δt = 0.1ms, and passed to the Langevin simulation (section 3.4).

3.4 Langevin Simulation

We used a Langevin simulation written in C++ similar to that in ref (*S14*), but with simplified rotor dynamics, to produce simulated revolution records for a bead undergoing rotational Brownian motion attached to the motor via an elastic linker. In each simulation step of length Δt, rotor position was updated following:

$$\theta_{rotor}(t+\Delta t) = \theta_{rotor}(t) + V_{rotor}(t)\Delta t;$$

where $V_{rotor} = \frac{V_0(N_{CCW}(t) - 17)}{17}$ according to the model outlined in the main text, and $N_{CCW}(t)$ is the output of the Monte-Carlo simulation of conformational spread in the rotor (section 3.3). Bead position is updated by introducing a Wiener process:

$$\theta_{bead}(t+\Delta t) \approx \theta_{bead}(t) + \frac{\Gamma}{\zeta_{bead}}\Delta t + Z\frac{1}{\kappa}\left(1 - e^{-2\frac{\kappa . k_B T}{\zeta_{bead}}\Delta t}\right);$$

here Z is a normal random variable with zero mean and unit variance (*S15*), ζ_{bead} is the drag coefficient of the bead, Γ is the torque delivered through the flexible linkage in the hook/flagellum that can be modeled by assuming an ideal elastic spring:

$$\Gamma = \kappa(\theta_{rotor} - \theta_{bead})\,;$$

κ is the experimentally determined stiffness of the hook/flagellum (*S5*). Note that the last term reduces to the more common $Z\sqrt{2D_{bead}\Delta t}$ in the limit of small Δt, with the corrected term above used to reduce computation time by allowing larger values of Δt (0.1ms).

Angles θ_{bead} obtained from simulations were split into 30 s records and analyzed identically to experimental bead-angle records. Simulation records were binned by CW bias rather than the underlying value of $c/c_{0.5}$.

3.5 Choice of parameters E_A and E_J

A 2-dimensional parameter space search was conducted to find suitable values for E_A and E_J. MATLAB's fminsearch function was used to locate a stable minimum of the cost function $\sum_q \left(S_q - E_q\right)^2 / E_q^2$, where S and E denote simulation and experimental mean values respectively for the switch time ($q=1$) and mean rotational state interval length ($q=2$). E_1 (18.72 ms) was obtained from all 3579 switches analyzed, and E_2 (0.75 s) from 448 intervals from the records where the CW bias was between 0.45 and 0.55. S_q were obtained from identical analysis of 50 separate 30 s simulations with the parameter $c/c_{0.5}$ set to 1 to give an average bias of 0.5. Starting values of $E_J = 4\ k_BT$ and $E_A = 1\ k_BT$ were used, based on the simulations of reference *S*9. Final values were $E_J = 4.13\ k_BT$ and $E_A = 0.66\ k_BT$. Note that these fit values are sensitive to the parameters fixed in section 3.1, such that changing any of ω_a, ω_b, λ_a, λ_b would alter the fit parameters for E_A and E_J.

3.6 Simulated hook-bead response distribution

We carried out another Langevin simulation to investigate the hook-bead response time distribution. Instead of calculating rotor speed with the conformational spread model of the flagellar switch, we simulated rotation as a 400 steps/revolution Poisson stepper (*S16*) that makes instantaneous directional switches at a fixed frequency. We used the speed observed in experiments (0.5 μm bead average 120 Hz, 0.35 μm bead average 160 Hz) as a control parameter of the stepping frequency. The simulation outputs a bead-angle record. We applied the experimental switch duration measurement algorithm to these simulated records to determine the predicted response of 0.5 μm and 0.35 μm beads.

Measured switch durations were assumed to be the sum of the hook-bead response time and the time required by the switch mechanism to reverse rotation. We obtained the

distribution of the latter component by performing a deconvolution of the experimentally determined distribution and the simulated hook-bead response time distribution, both fitted with gamma functions using maximum likelihood estimation. This procedure was carried out on the 0.0-0.3 CW bias bins (the largest data sets) for both 0.5 μm and 0.35 μm bead datasets (Fig. S12).

The hook/flagellum stiffness value used in the simulations is a conservative estimate taken from reference *S5*. Therefore, the hook-bead response time simulated here is unlikely to be an underestimate. Furthermore, even with considerably larger hook compliance, the switch time distribution is far narrower than the observed spread of switch times in a single cell record. To explain the observed peak in the experimental distribution by means of only the hook-bead response, the hook stiffness required would need to vary from hook to hook across the range 1/10-1/100 of the published value.

3.7 Missed events analysis

Concern over whether very short intervals were missed due to experimental noise and filtering was addressed by analyzing the simulation protomer records, which are free from noise and filtering, with an analogous interval measurement algorithm to that described in section 2.3, but with thresholds set to detect transitions between 0 and 34 active subunits. These data are found to be exponentially distributed with rate constants in very good agreement with the simulation distributions (Fig. S13). This approach is equivalent to simulation techniques used for determining the significance of missed events in ion channel record analysis (*S17*), and suggests that missed events are unlikely to be an issue in the experimental data.

4. Simulation movie

The movie shows a simulation of the conformational spread model of the bacterial flagellar switch for 60 ms of activity. The left panel illustrates the state of the simulated complex graphically, while the right panel shows the numbers of active protomers and bound CheY-P molecules. Switches typically occur via a single nucleation of a new domain, followed by conformational spread of the domain, which follows a biased random walk until it either encompasses the entire ring, or collapses back to the previous coherent state.

B) Supporting Online Material Figures

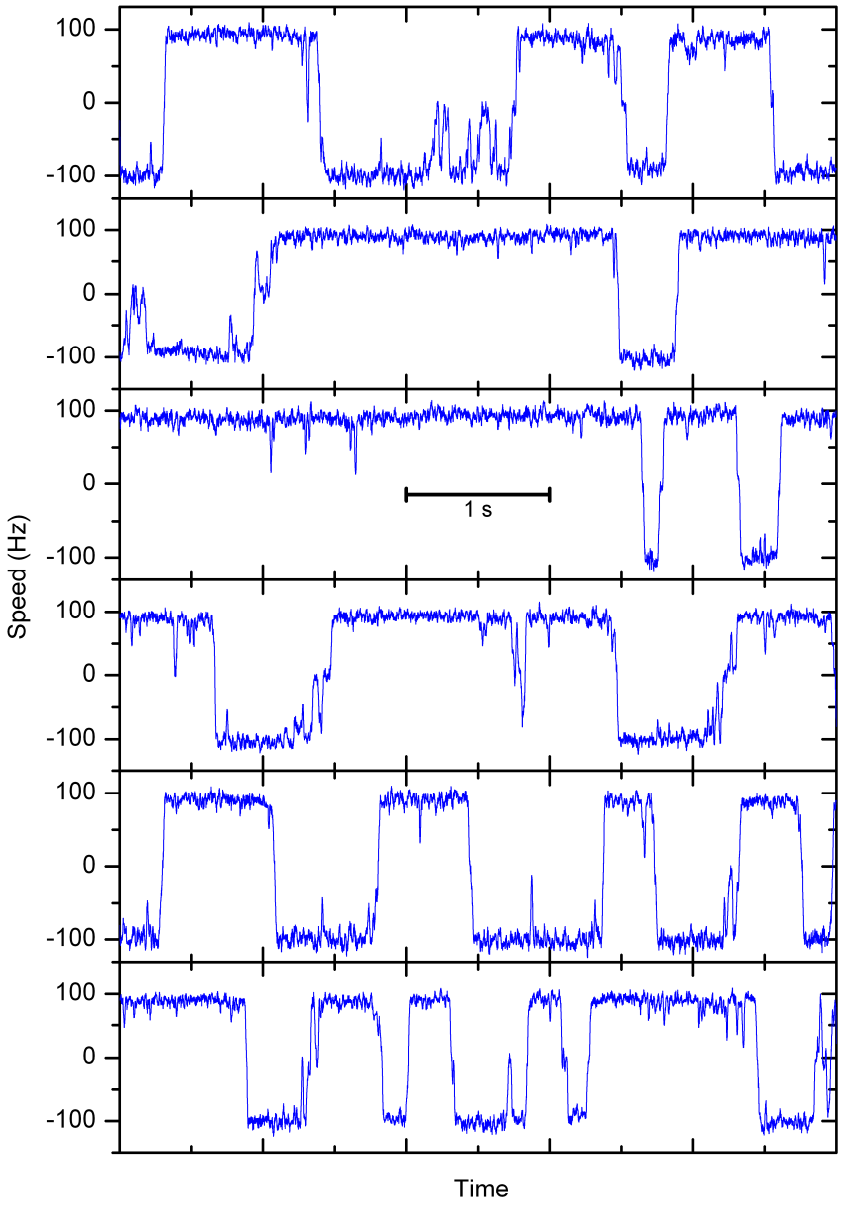

Figure S1. The full 30 s trace from the cell shown in Fig. 2A, median filtered (100 points) to reduce noise. The trace is split into 5 s sections top to bottom.

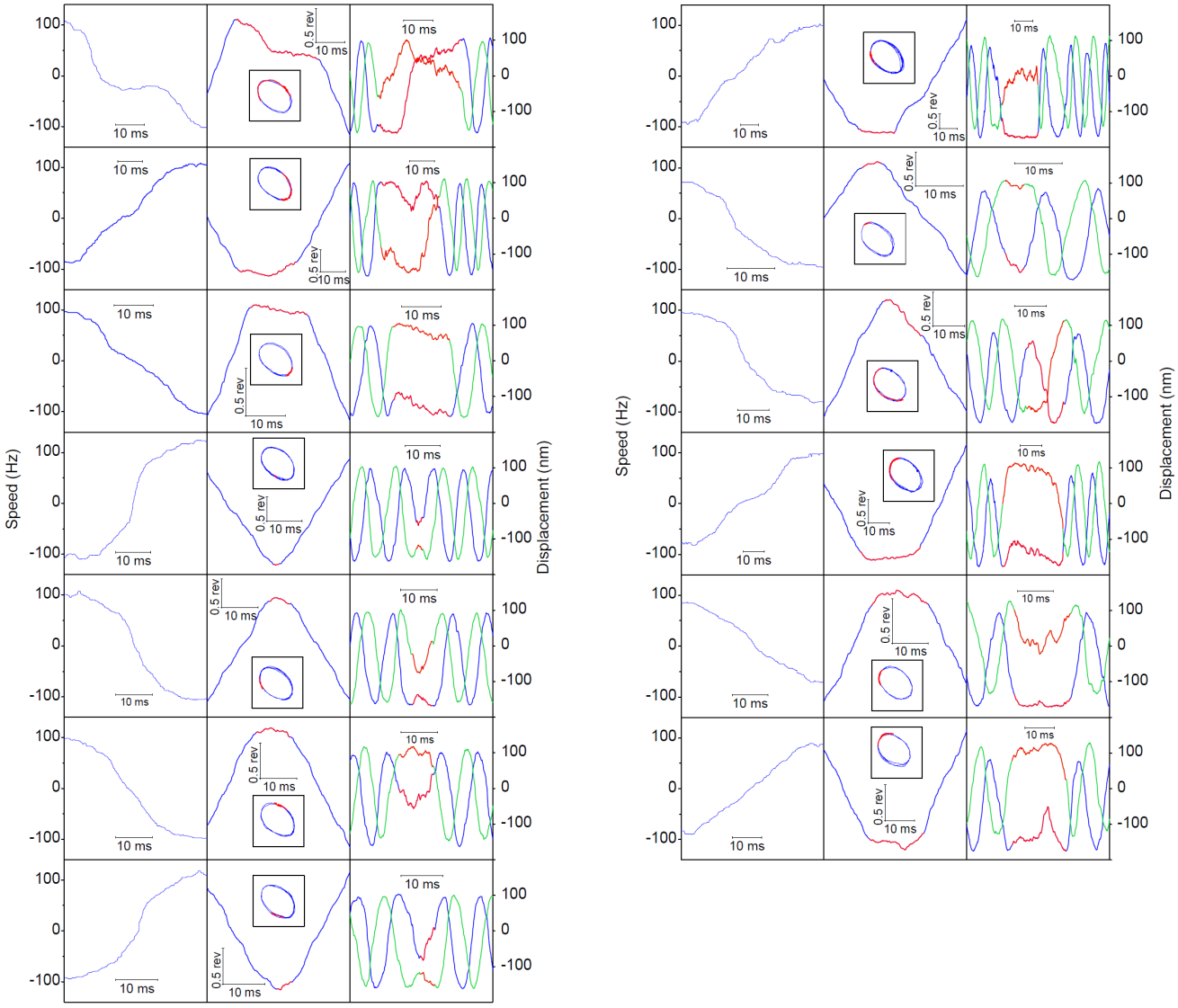

Figure S2. All of the 13 complete switches measured from a single cell record, plotted as in Figure 2B-D. Switch durations from top to bottom are 27.9 ms, 22.9 ms, 14.2 ms, 1.6 ms, 5.4 ms, 9.2 ms, 3.4 ms, 19.8 ms, 3.9 ms, 11.7 ms, 28.7 ms, 15.6 ms, 18.4 ms.

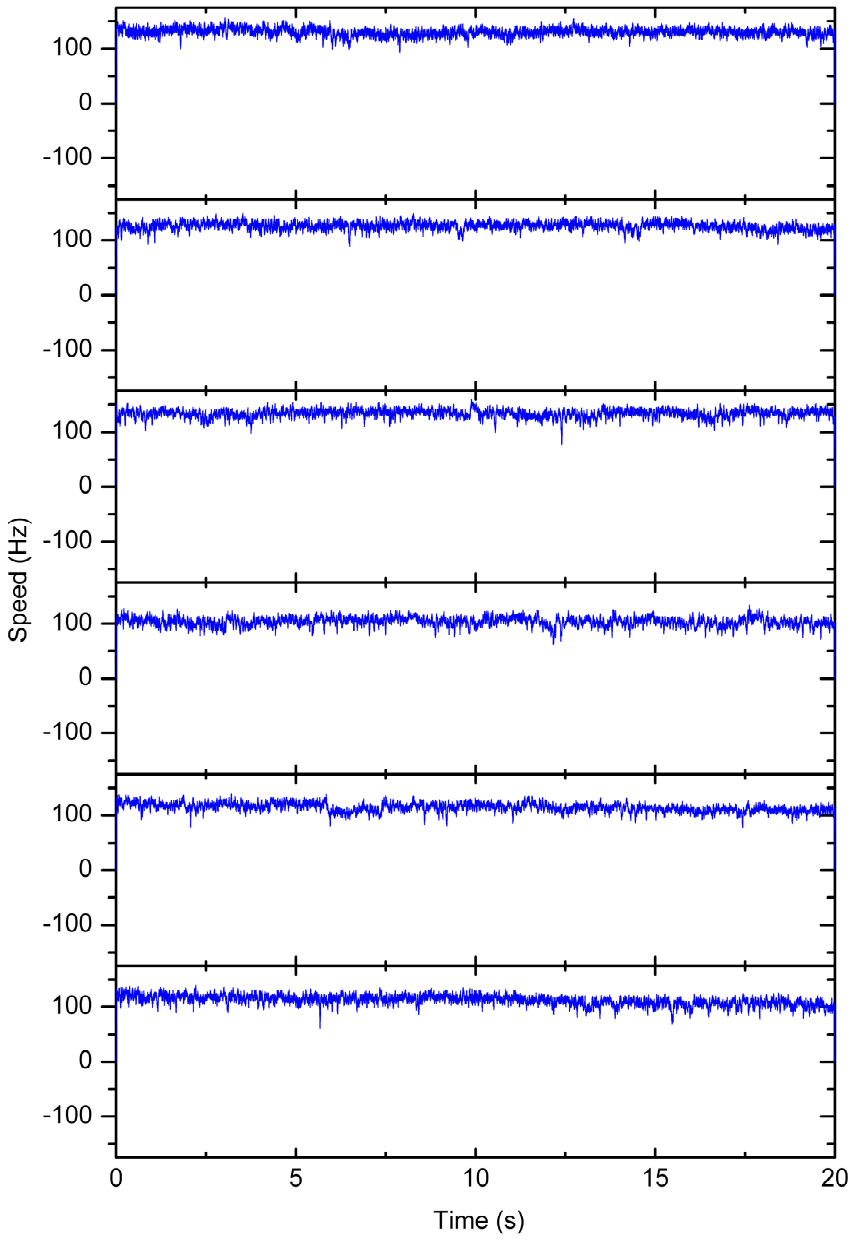

Figure S3. 20 s speed records from six different cells of an *E. coli* non-switching strain (KAF95 (*ΔcheY*, *fliC726*), pFD313 (pFD313 (*fliC*st, Ap^{R}) (*S1*)). Transient fluctuations in speed are absent indicating that the bead assay is not susceptible to mechanical hindrances and that transient fluctuations are dependent on motor switching.

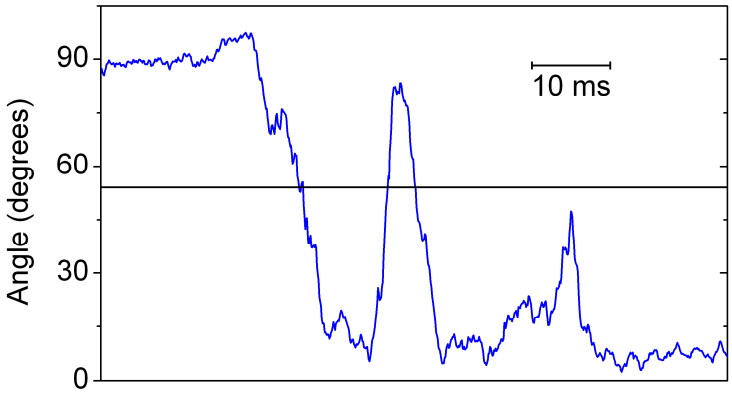

Figure S4. Non-instantaneous complete and incomplete switching observed using an optical trap to stall bead-pairs attached to the motor. Bead-pair angle is shown in blue, trap angle in black. CCW motor operation corresponds to about 90º and CW operation to about 10º. Angles were sampled at 10 kHz and are shown without filtering.

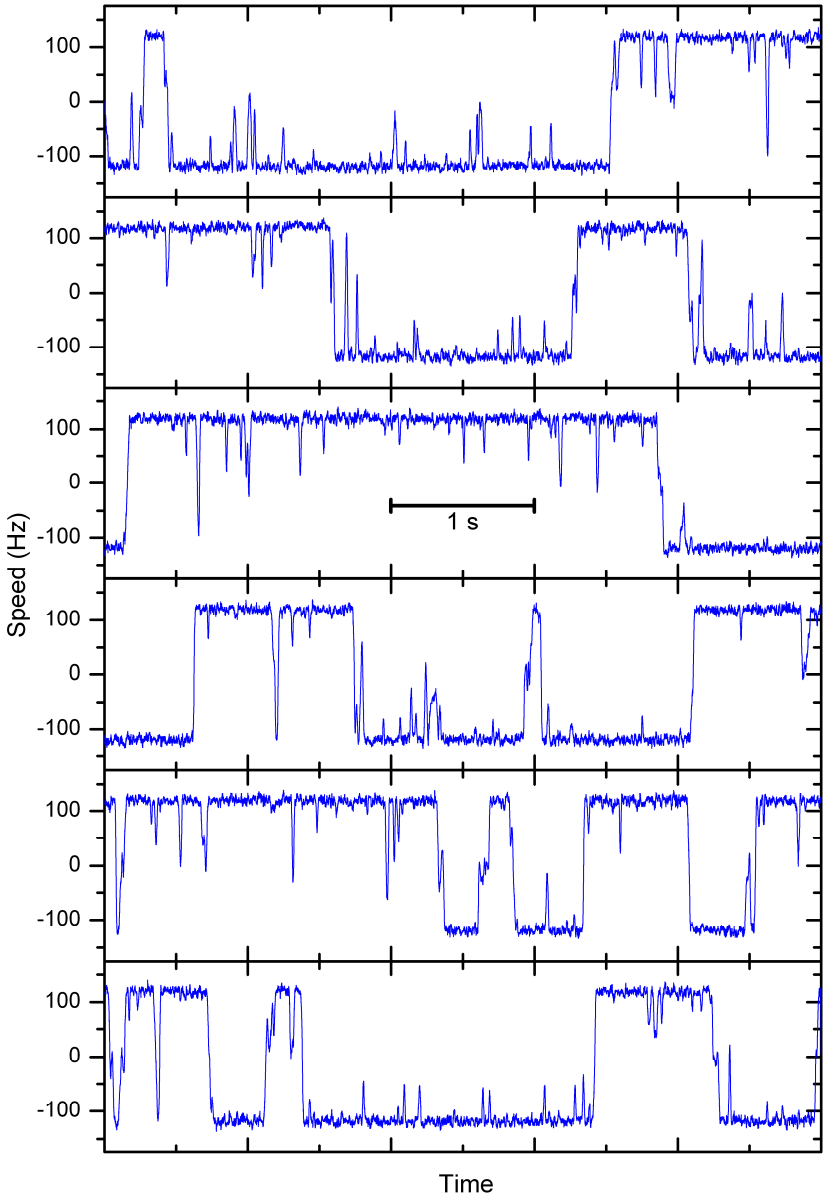

Figure S5. The full 30 s record from the simulation shown in Fig. 3B, median filtered (100 points) to reduce noise. The trace is split into 5 s sections top to bottom.

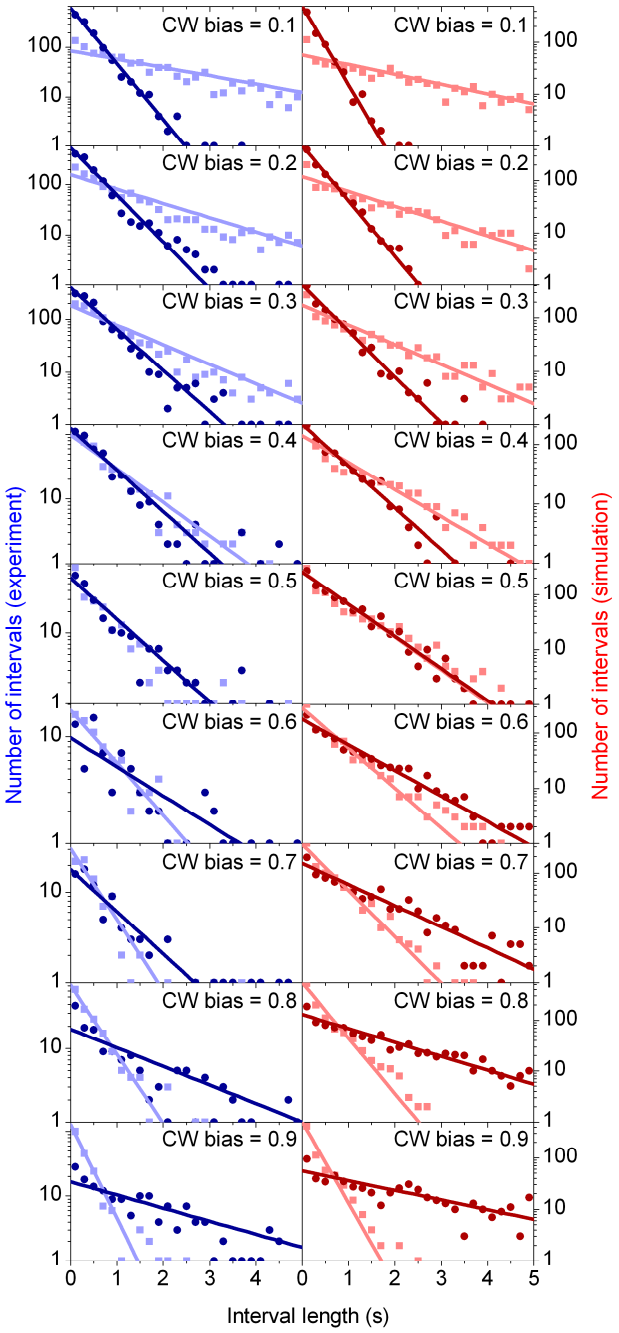

Figure S6. Distribution of intervals between complete switches across the full bias range for experiment (blue) and simulation (red) datasets. Light squares represent CCW data and dark circles represent CW data. Lines are exponential maximum likelihood fits. The total number of experimental intervals in each CW bias bin is as follows: 0.1 ± 0.05, 2335 intervals; 0.2 ± 0.05, 2462 intervals; 0.3 ± 0.05, 2174 intervals; 0.4 ± 0.05, 824 intervals; 0.5 ± 0.05, 448 intervals; 0.6 ± 0.05, 156 intervals; 0.7 ± 0.05, 167 intervals; 0.8 ± 0.05, 323 intervals; 0.9 ± 0.05, 369 intervals.

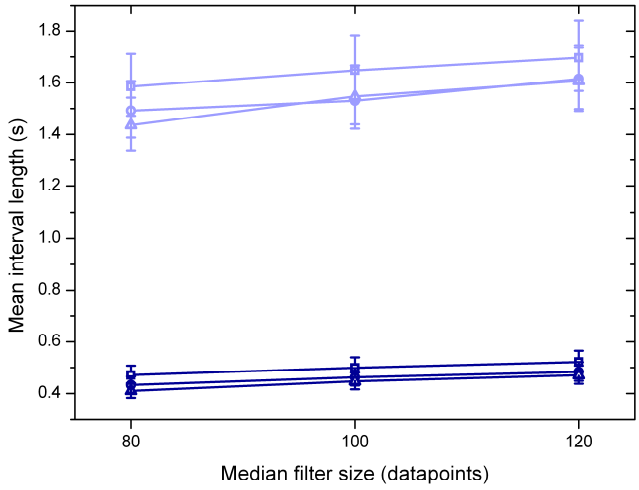

Figure S7. Robustness of interval-finding algorithm to 20% variations in filter and threshold level. Threshold levels are α = 0.83 (squares), 0.67 (circles) and 0.59 (triangles) for CCW (light blue) and CW (dark blue) data. Error bars are 95% confidence intervals.

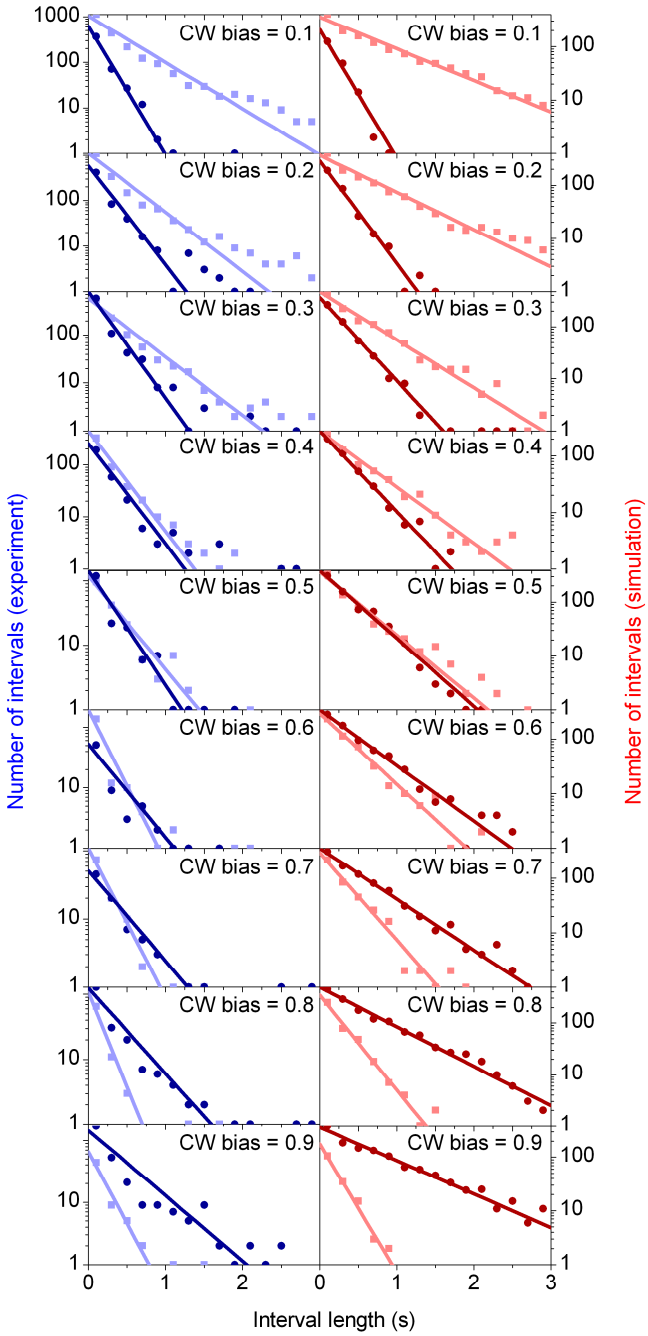

Figure S8. Distribution of intervals between incomplete switches for β=1/3 across the full bias range for experiment (blue) and simulation (red) datasets. Light squares represent CCW data and dark circles represent CW data. Lines are exponential maximum likelihood fits. The total number of experimental intervals in each CW bias bin is as follows: 0.1 ± 0.05, 2714 intervals; 0.2 ± 0.05, 2423 intervals; 0.3 ± 0.05, 1829 intervals; 0.4 ± 0.05, 794 intervals; 0.5 ± 0.05, 357 intervals; 0.6 ± 0.05, 241 intervals; 0.7 ± 0.05, 193 intervals; 0.8 ± 0.05, 288 intervals; 0.9 ± 0.05, 361 intervals.

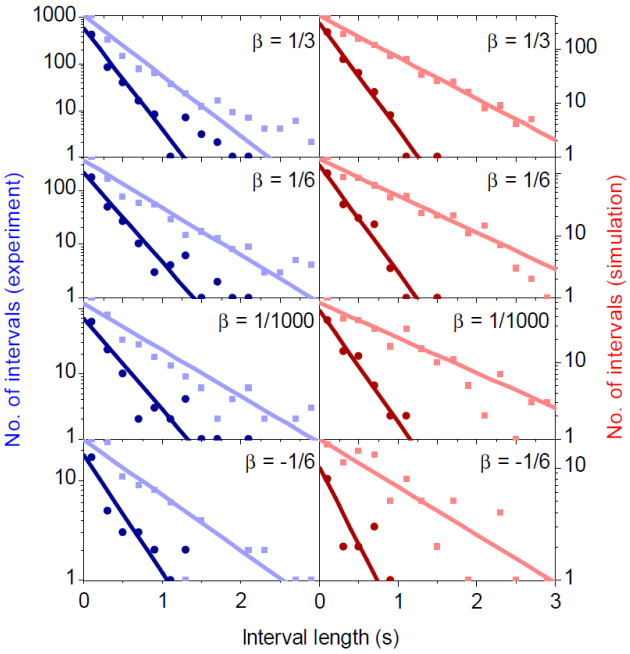

Figure S9. Distribution of intervals between incomplete switches for the CW bias bin with the largest amount of data (0.2±0.05), with varying β for experiment (blue) and simulation (red) datasets. Light squares represent CCW data and dark circles represent CW data. Lines are exponential maximum likelihood fits.

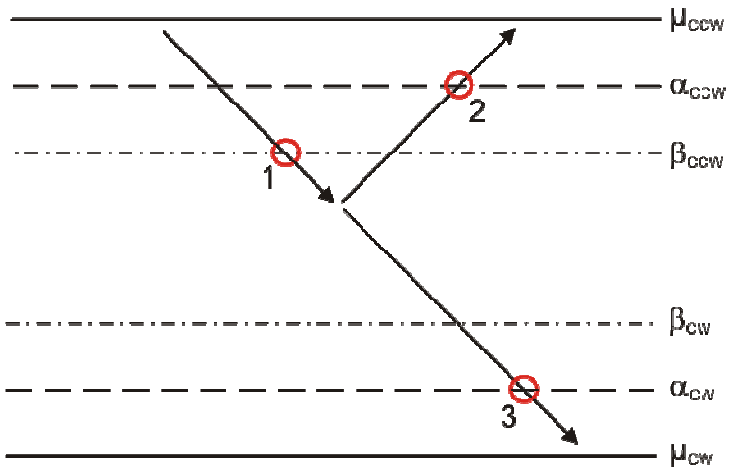

Figure S10. Thresholding scheme for complete and incomplete switching. Shown is the scheme for events starting from the CCW rotational state above α_{CCW}. Only those crossings marked by circles are recorded. Crossing β_{CCW} signals a possible incomplete switch (1). An incomplete switch is recorded if crossing α_{CCW} occurs before crossing α_{CW} (2). Otherwise a complete switch is recorded (3), marking the end of a CCW interval and the start of a CW interval. The CW scheme is defined analogously.

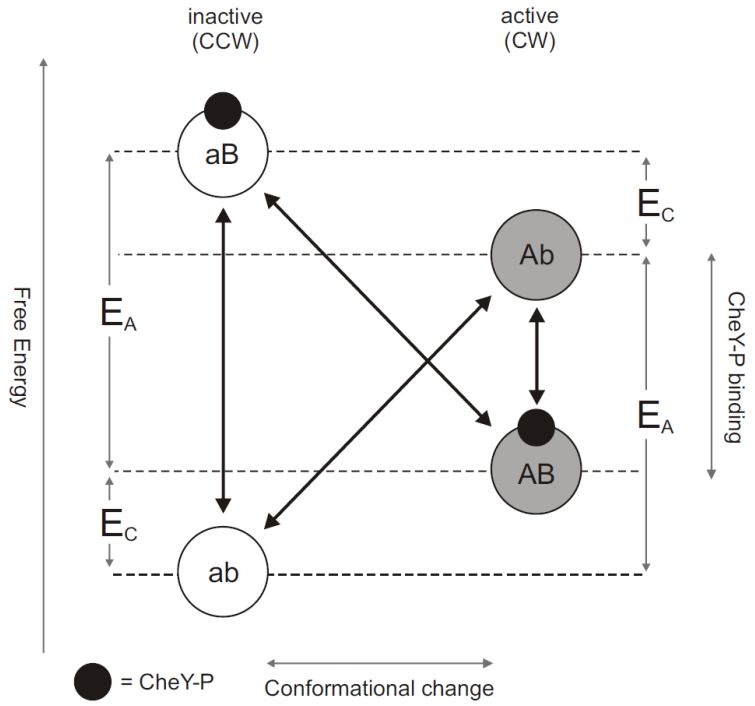

Figure S11. Free energy diagram for the conformational spread reaction scheme, excluding free energy due to the conformation of neighboring protomers (E_J, see Fig. 1C). This is a generalized version of that shown in Fig. 1C. The free energy of conformational change is $\pm E_A$. The free energy of CheY-P binding is dependent on the CheY-P concentration as shown, with $E_C = - log_e(c/c_{0.5})$. If $E_C > 0$, the inactive state becomes more highly populated and hence CW bias < 0.5, while $E_C < 0$ similarly implies CW bias > 0.5.

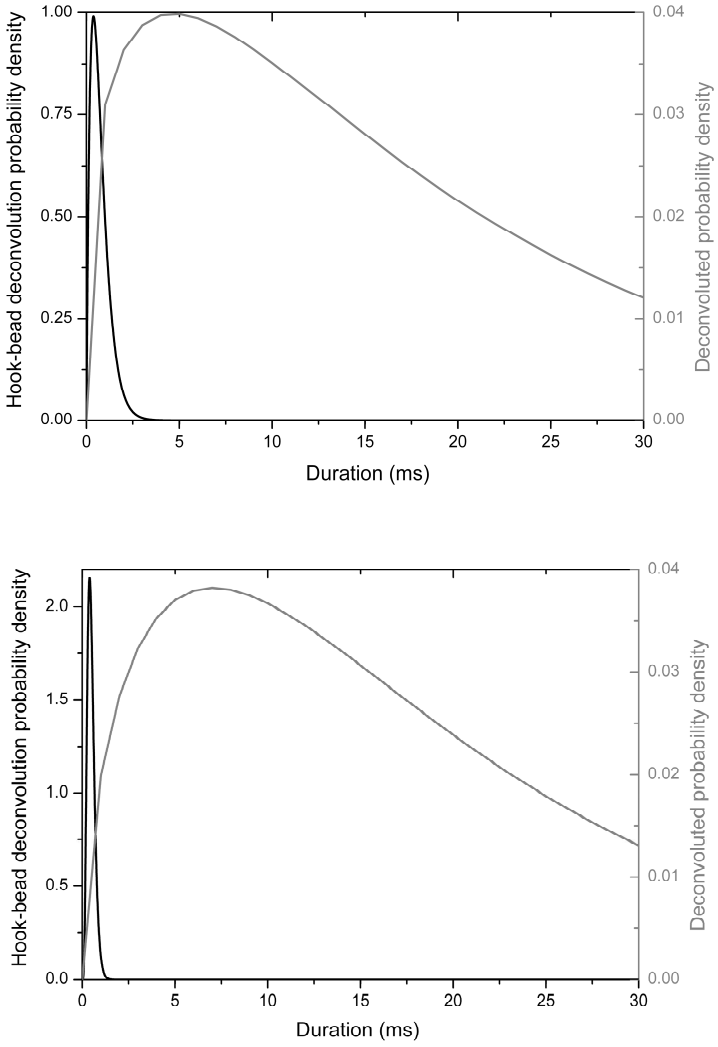

Figure S12. Simulated hook-bead response time distribution (black) and a deconvolution between this distribution and the experimental switch time distribution (grey), for 532nm bead (top) and 350nm bead (bottom) datasets. The theoretical hook-bead response time distribution has too small a mean and variance to account for the experimentally observed distribution and the deconvoluted switch duration remains broadly distributed. The similarity between the deconvoluted distributions for both datasets demonstrates the independence of the underlying distribution on bead size.

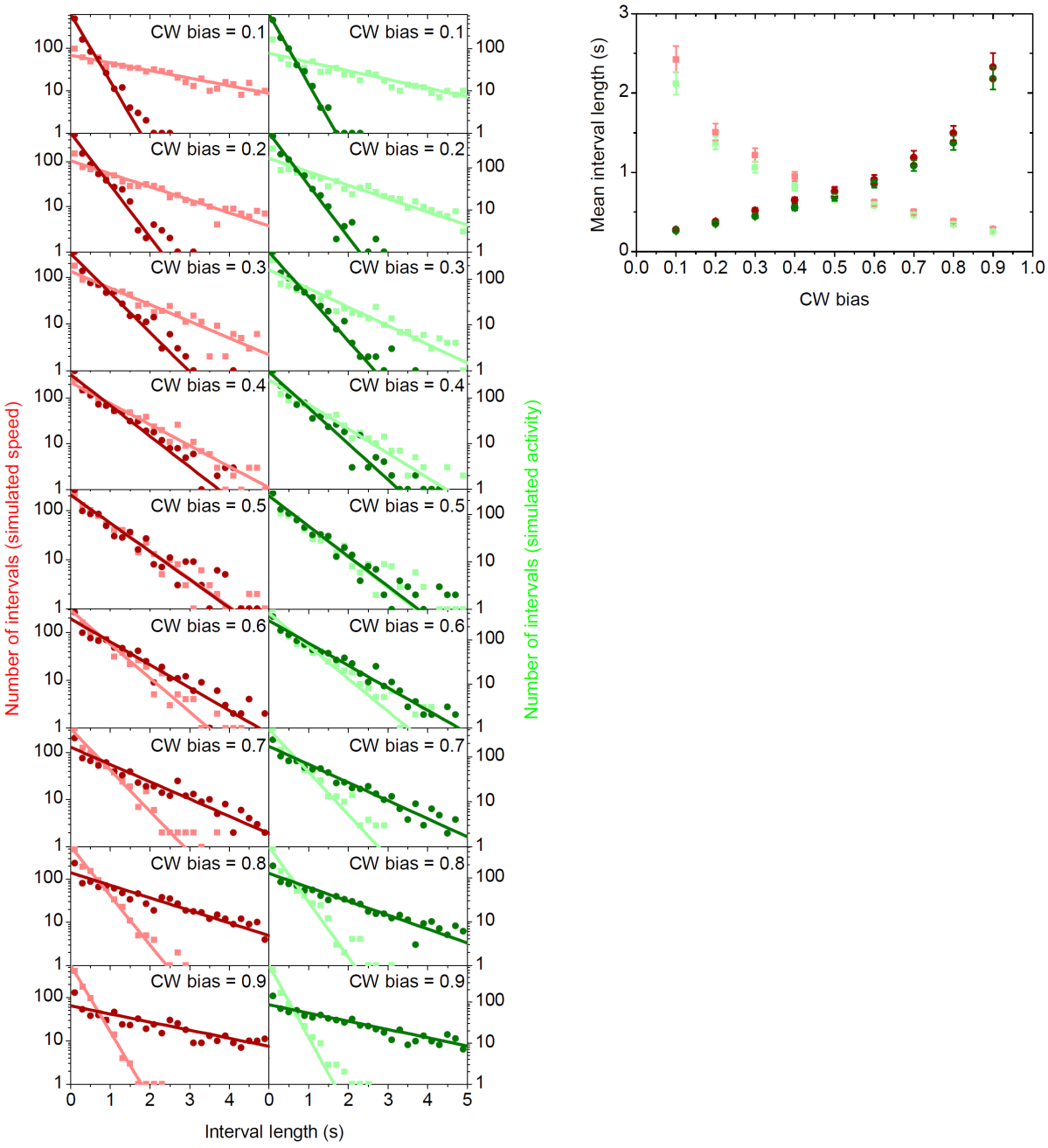

Figure S13. Left: Interval distributions from simulation records (red) and protomer records (green) for CCW data (light squares) and CW data (dark circles). Lines are exponential maximum likelihood fits. Right: the corresponding distribution fit parameters. Error bars are 95% confidence intervals.

C) Supporting Material References

S1. H. C. Berg, L. Turner, *Biophys. J.* **65**, 2201 (1993).
S2. Y. Sowa *et al.*, *Nature* **437**, 916 (2005).
S3. E. Korobkova, T. Emonet, J. M. G. Vilar, T. S. Shimizu, P. Cluzel, *Nature* **428**, 574 (2004).
S4. E. A. Korobkova, T. Emonet, H. Park, P. Cluzel, *Phys. Rev. Lett.* **96**, 058105 (2006).
S5. S. M. Block, D. F. Blair, H. C. Berg, *Nature* **338**, 514 (1989).
S6. W. S. Ryu, R. M. Berry, H. C. Berg, *Nature* **403**, 444 (2000).
S7. I. R. Lapidus, M. Welch, M. Eisenbach. *J. Bacteriol.* **170**, 3627 (1988).
S8. R. Yasuda, H. Noji, M. Yoshida, K. Kinosita Jr., H. Itoh, *Nature* **410**, 898 (2001).
S9. T. A. J. Duke, N. Le Novère, D. Bray, *J. Mol. Biol.* **308**, 541 (2001).
S10. B. Hille, *Ionic Channels of Excitable Membranes* (Sinauer Associates Inc, Sunderland, MA., ed. 2, 1992)
S11. V. Sourjik, H. C. Berg, *Proc. Natl. Acad. Sci. U.S.A.* **99**, 12669 (2002).
S12. C. J. Camacho, S. R. Kimura, C. DeLisi, S. Vajda, *Biophys. J.* **78**, 1094 (2000).
S13. M. Matsumoto, T. Nishimura, in *ACM Transactions on Modeling and Computer Simulation*, vol. 8, no. 1, 1998, pp. 3-30.
S14. J. Xing, F. Bai, R. Berry, G. Oster, *Proc. Natl. Acad. Sci. U.S.A.* **103**, 1260 (2006).
S15. H. Risken, *The Fokker-Planck Equation: Methods of Solutions and Applications* (Springer-Verlag, New York, 1996).
S16. A. D. Samuel, H. C. Berg, *Proc. Natl. Acad. Sci. U.S.A.* **92**, 3502 (1995).
S17. F. Qin, L. Li, *Biophys. J.* **87**, 1657 (2004).